# Entrance channel dynamics of hot and cold fusion reactions leading to superheavy elements

A. S. Umar,[1] V. E. Oberacker,[1] J. A. Maruhn,[2] and P.-G. Reinhard[3]
[1]*Department of Physics and Astronomy, Vanderbilt University, Nashville, Tennessee 37235, USA*
[2]*Institut für Theoretische Physik, Goethe-Universität, D-60438 Frankfurt am Main, Germany*
[3]*Institut für Theoretische Physik, Universität Erlangen, D-91054 Erlangen, Germany*
(Received 20 April 2010; published 17 June 2010)

We investigate the entrance channel dynamics for the reactions $^{70}$Zn + $^{208}$Pb and $^{48}$Ca + $^{238}$U by using the fully microscopic time-dependent Hartree-Fock theory coupled with a density constraint. We calculate excitation energies and capture cross sections relevant for the study of superheavy formations. We discuss the deformation dependence of the ion-ion potential for the $^{48}$Ca + $^{238}$U system and perform an alignment angle averaging for the calculation of the capture cross section. The results show that this approach can generate results in good agreement with experiments and other theories.

DOI: 10.1103/PhysRevC.81.064607 PACS number(s): 21.60.Jz, 25.70.Jj, 27.90.+b

## I. INTRODUCTION

One of the most fascinating research areas involving low-energy nuclear reactions is the search for superheavy elements. Experimentally, two approaches have been used for the synthesis of these elements, one utilizing closed-shell nuclei with lead-based targets (cold fusion) [1,2], the other utilizing deformed actinide targets with $^{48}$Ca projectiles (hot fusion) [3–5]. While both methods have been successful in synthesizing new elements, the evaporation residue cross sections of the hot fusion reactions were found to be as much as three times larger than those of the cold fusion ones. To pinpoint the root of this difference, it is important to understand the details of the entrance channel dynamics of these systems, since the properties of the dinuclear system at the capture point will strongly influence the outcome of the reaction. For light- and medium-mass systems, the capture cross section may be considered to be the same as that for complete fusion, whereas for heavy systems leading to superheavy formations, the evaporation residue cross section is dramatically reduced due to the quasifission and fusion-fission processes, thus, making the capture cross section essentially be the sum of these two cross sections. What is also difficult to ascertain is the configuration of the composite system, namely, whether the system has a single-center compoundlike configuration or a dinuclear configuration accompanied by particle exchange. Most dynamical models [6–11] argue that, for heavy systems, a dinuclear complex is formed initially, and the barrier structure and the excitation energy of this precompound system will determine its survival by breaking up via quasifission. Furthermore, if the nucleus survives this initial state and evolves to a compound system, it can still fission due to its excitation. Recent microscopic calculations have shown that the temperature (excitation energy) of the compound systems strongly alters the barrier structures of potential-energy surfaces, with implications of very different fusion-fission cross sections than those predicted by zero-temperature calculations [12].

It is generally acknowledged that the time-dependent Hartree-Fock (TDHF) theory provides a useful foundation for a fully microscopic many-body theory of low-energy heavy-ion reactions [13]. Recent three-dimensional (3D) TDHF calculations with no symmetry assumptions and that use modern Skyrme forces have been shown to accurately reproduce phenomena determined by the early stages of the heavy-ion dynamics [14–16]. Recently, we have developed the density-constrained (DC) TDHF (DC-TDHF) method [17], which is based on the generalization of the DC method developed earlier [18]. We have shown that, by using the DC-TDHF method, ion-ion potential barriers can be accurately produced in most cases [19–21], as these calculations also depend on early stages of the ion-ion dynamics. Furthermore, one-body energy dissipation extracted from the TDHF for low-energy fusion reactions was found to be in agreement with the friction coefficients based on the linear-response theory as well as those in models where the dissipation was specifically adjusted to describe experiments [22]. All of these new results suggest that TDHF dynamics may provide a good description of the early stages of heavy-ion collisions.

Recently, we have also introduced an approach to extract excitation energies directly from full microscopic TDHF calculations [23]. In this paper, we perform TDHF calculations accompanied by DC calculations for $^{70}$Zn + $^{208}$Pb and $^{48}$Ca + $^{238}$U systems, which represent typical examples of cold and hot fusion reactions, respectively, leading to superheavy formation. In addition to calculating the excitation energy at the capture point, we also investigate the capture cross section and try to elucidate the differences between these two reactions.

## II. THEORETICAL OUTLINE

In this section, we will discuss issues pertaining to the application of TDHF for studying collisions involving heavy-reaction partners.

### A. TDHF dynamics

It is generally accepted that TDHF theory is a candidate for a microscopic theory that may provide a unified approach for the description of diverse physical phenomena such as fusion, deep-inelastic collisions, dinuclear and compound-nucleus formation, and, possibly, fission. Since TDHF is based on the independent-particle approximation, it can be

 

interpreted as the semiclassical limit of a fully quantal theory, thus, allowing a connection to macroscopic coordinates and providing insight about the collision process. In this sense, the TDHF dynamics can only compute the semiclassical trajectories of the collective moments of the composite system as a function of time. The presence of residual interaction, absent in TDHF, may produce fluctuations and correlations, which affect the mean values of these trajectories.

For TDHF collisions of light- and medium-mass systems as well as highly mass-asymmetric systems, fusion generally occurs immediately above the Coulomb barrier, while in heavier systems, there is an energy range above the barrier, where fusion does not occur. This phenomenon is the microscopic analog of the macroscopic *extrapush* threshold [24] and has been recently studied for TDHF collisions involving heavy- and nearly symmetric-reaction partners [25]. In the lower part of this energy range, deep-inelastic collisions are dominant, while at slightly higher energies, the system develops a long-lived and pronounced neck reminiscent of a dinuclear configuration. The outcome of these long-lived configurations is uncertain due to the absence of quantum-decay processes and transitions. For these systems, TDHF results in a compact configuration only for energies considerably above the static potential-energy surface. However, despite the high-energy, single-particle friction can quickly absorb this energy and can lead to a configuration that may be considered a thermal doorway state. As long as the average single-particle excitation energy per nucleon in this doorway state is less than the shell energy (about 4–8 MeV), the details of the ground-state potential-energy surface are still felt, and shell-correction energies influence the TDHF dynamics. It is precisely for this reason, that the DC-TDHF approach allows us to reproduce ion-ion interaction barriers for heavy-ion collisions.

### B. DC-TDHF and excitation energy

In the DC-TDHF approach [17], the TDHF time evolution takes place with no restrictions. At certain times during the evolution, the instantaneous density is used to perform a static Hartree-Fock (HF) minimization while holding the neutron and proton densities constrained to be the corresponding instantaneous TDHF densities. In essence, this provides us with the TDHF dynamical path in relation to the multi-dimensional static energy surface of the combined nuclear system. The advantages of this method in comparison to other mean-field-based microscopic methods such as the constrained HF (CHF) method are obvious. First, there is no need to introduce artificial constraining operators, which assume that the collective motion is confined to the constrained phase space: Second, the static adiabatic approximation is replaced by the dynamical analog, where the most energetically favorable state is obtained by including sudden rearrangements, and the dynamical system does not have to move along the valley of the potential-energy surface. In short, we have a self-organizing system, which selects its evolutionary path by itself by following the microscopic dynamics. All of the dynamical features included in the TDHF are naturally included in the DC-TDHF calculations. These effects include neck formation, mass exchange, internal excitations, deformation effects to all orders, as well as the effect of nuclear alignment for deformed systems. In the DC-TDHF method, the ion-ion interaction potential is given by

$$V(R) = E_{\rm DC}(R) - E_{A_1} - E_{A_2}, \tag{1}$$

where $E_{\rm DC}$ is the DC energy at the instantaneous separation $R(t)$, while $E_{A_1}$ and $E_{A_2}$ are the binding energies of the two nuclei obtained with the same effective interaction. In writing Eq. (1), we have introduced the concept of an adiabatic reference state for a given TDHF state. The difference between these two energies represents the internal energy. The adiabatic reference state is the one obtained via the DC calculation, which is the Slater determinant with the lowest energy for the given density with a vanishing current and which approximates the collective potential energy [18]. We would like to emphasize again that this procedure does not affect the TDHF time evolution and contains no free parameters or normalization.

Ion-ion interaction potentials calculated using the DC-TDHF correspond to the configuration attained during a particular TDHF collision. For light- and medium-mass systems as well as for heavier systems for which fusion is the dominant reaction product, the DC-TDHF gives the fusion barrier with an appreciable but relatively small energy dependence. On the other hand, for reactions that lead to superheavy systems, fusion is not the dominant channel at barrier top energies. Instead, the system sticks in some dinuclear configuration with possible breakup after exchanging a few nucleons. The long-time evolution to breakup is beyond the scope of the TDHF due to the absence of quantum-decay processes and transitions. As we increase the energy above the barrier, this phenomenon gradually changes to the formation of a truly composite object. This is somewhat similar to the extrapush phenomenon discussed in phenomenological models. For this reason, the energy dependence of the DC-TDHF interaction barriers for these systems is not just due to the dynamical effects for the same final configuration but actually represents different final configurations.

The calculation of the excitation energy is achieved by dividing the TDHF motion into a collective and intrinsic part [23]. The major assumption in achieving this goal is to assume that the collective part is primarily determined by the density $\rho(\mathbf{r}, t)$ and the current $\mathbf{j}(\mathbf{r}, t)$. Consequently, the excitation energy can be formally written as

$$E^*(t) = E_{\rm TDHF} - E_{\rm coll}(\rho(t), \mathbf{j}(t)), \tag{2}$$

where $E_{\rm TDHF}$ is the total energy of the dynamical system, which is a conserved quantity, and $E_{\rm coll}$ represents the collective energy of the system. In the next step, we break up the collective energy into two parts,

$$E_{\rm coll}(t) = E_{\rm kin}(\rho(t), \mathbf{j}(t)) + E_{\rm DC}(\rho(t)), \tag{3}$$

where $E_{\rm kin}$ represents the kinetic part and is given by

$$E_{\rm kin}(\rho(t), \mathbf{j}(t)) = \frac{m}{2} \int d^3r\, \mathbf{j}^2(t)/\rho(t), \tag{4}$$

which is asymptotically equivalent to the kinetic energy of the relative motion $\frac{1}{2}\mu\dot{R}^2$, where $\mu$ is the reduced mass and $R(t)$ is the ion-ion separation distance. The dynamics of the ion-ion

separation $R(t)$ is provided by an unrestricted TDHF run, thus, allowing us to deduce the excitation energy as a function of the distance parameter $E^*(R)$.

## III. RESULTS

Calculations were done in 3D geometry and by using the full Skyrme force (SLy4) [26] without the c.m. correction as described in Ref. [27]. We have performed DC calculations every 20 time steps. For the calculation of the ion-ion separation distance $R$, we use the hybrid method, which relates the coordinate to the quadrupole moment for small $R$ values, as described in Ref. [21]. The accuracy of the DC calculations is commensurate with the accuracy of the static calculations.

### A. $^{48}$Ca + $^{238}$U system

As an example of superheavy formation from a hot fusion reaction, we have studied the $^{48}$Ca + $^{238}$U system. HF calculations produce a spherical $^{48}$Ca nucleus, whereas $^{238}$U has a large axial deformation. The large deformation of $^{238}$U is expected to strongly influence the interaction barriers for this system. This is shown in Fig. 1, which shows the interaction barriers $V(R)$ calculated by using the DC-TDHF method as a function of c.m. energy and for three different orientations of the $^{238}$U nucleus. The alignment angle $\beta$ is the angle between the symmetry axis of the $^{238}$U nucleus and the collision axis. Also shown in Fig. 1 is the point Coulomb potential corresponding to this collision. The deviations from the point Coulomb potential at large $R$ values are caused by the deformation of the $^{238}$U nucleus. We first notice that the barriers that correspond to the polar orientation ($\beta = 0^\circ$) of the $^{238}$U nucleus are much lower and peak at larger ion-ion separation distance $R$. On the other hand, the barriers that correspond to the equatorial orientation of $^{238}$U ($\beta = 90^\circ$) are much higher and peak at smaller $R$ values. For the intermediate values of $\beta$, the barriers rise rapidly as we increase the orientation angle from $\beta = 0^\circ$, as can be seen for $\beta = 45^\circ$. The rise in the barrier height as a function of increasing $\beta$ values is not linear but seems to rise more rapidly for smaller $\beta$ values. We also see that, for lower energies, central collisions with polar orientations of $^{238}$U are the only orientations that result in the sticking of the two nuclei, while the equatorial orientations of $^{238}$U result in a deep-inelastic collision. Also, shown in Fig. 1 are the experimental energies [4,5] for this reaction. We observe that all of the experimental energies are above the barriers obtained for the polar alignment of the $^{238}$U nucleus.

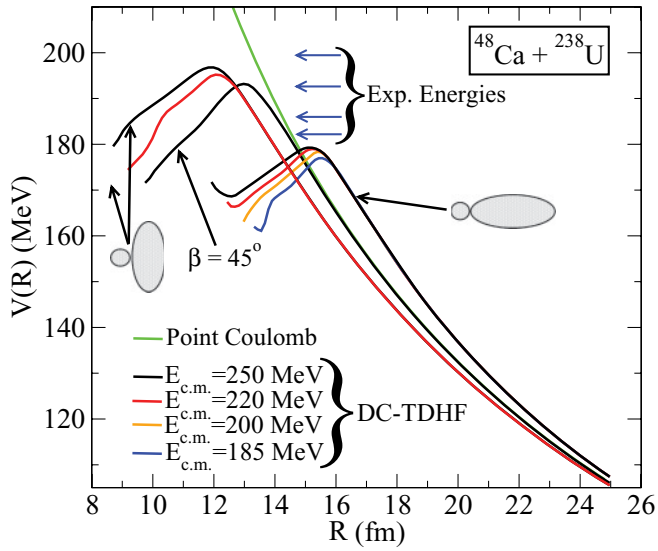


FIG. 1. (Color online) Potential barriers $V(R)$ for the $^{48}$Ca + $^{238}$U system obtained from DC-TDHF calculations using Eq. (1) as a function of $E_{c.m.}$ energy and for selected orientation angles $\beta$ of the $^{238}$U nucleus. Also shown are the experimental c.m. energies.

Furthermore, the potentials shown in Fig. 1 display a very strong energy dependence. Detailed analysis of the TDHF time evolution and density profiles show that, at lower c.m. energies and for central collisions, the polar configuration of $^{238}$U leads to a dinuclear system, where both nuclei maintain their cores and exchange nucleons. Noncentral collisions at these energies result in deep-inelastic fragments. As we mentioned earlier, for these low-energy collisions, the equatorial collisions result in deep-inelastic reaction products even for central collisions. At higher energies, the system forms a true composite with overlapping cores. These are the potentials that should be used for calculating capture cross sections.

For the formation of a superheavy system, the excitation energy carries great significance, since a high-excitation energy at the capture point would result in quasifission events, while high excitation of the compound nucleus will lead to fusion-fission. Many factors play a role in building up the excitation energy. As we have discussed in Sec. I, recent TDHF calculations suggest that during the early phase of the ion-ion collisions, TDHF theory may provide a good approximation for the transfer of the initial kinetic energy into internal and collective excitations via the dynamical evolution of shell effects. Naturally, the excitation also depends on other nuclear properties such as deformation and alignment, mass asymmetry in the entrance channel, and impact parameter. In Fig. 2, we show the excitation energy $E^*(R)$ as a function of c.m. energy and for two alignment angles ($\beta = 0^\circ$ and $\beta = 90^\circ$) of the $^{238}$U nucleus. The excitation energy curves start at zero excitation when the two nuclei are far apart, which also provides a test for the numerical accuracy of the calculation. We note that the system is excited much earlier during the collision process for the polar alignment of the $^{238}$U nucleus and has a higher excitation than the corresponding collision for the equatorial orientation. Only two curves are shown for the equatorial collision, since at lower energies, we have deep-inelastic collisions for this alignment. We note that the highest point reached for these excitation curves is chosen to be the point where the nuclei almost come to a stop inside the barrier, which corresponds to a nearly zero collective kinetic energy. Since this is determined during the initial phase of the collision, the dinuclear system is not in thermal equilibrium. However, the system essentially oscillates about this point. For energies for which the collision outcome is capture, this would be the excitation energy at the capture point. Calculation of separate fragment excitation energies at the capture point is not possible because of technical reasons (in deriving the Skyrme energy functional, many integrations by parts are done

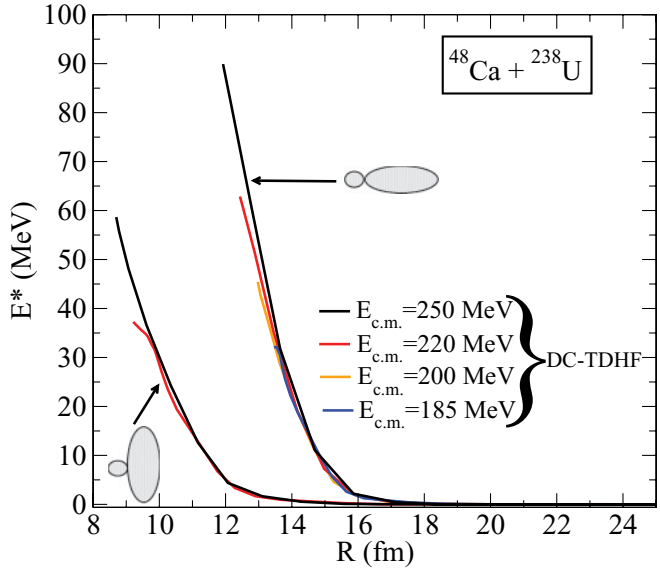


FIG. 2. (Color online) Excitation energy $E^*(R)$ in a central collision for various $E_{\text{c.m.}}$ energies and for alignment angles $\beta = 0^\circ$ and $\beta = 90^\circ$ of the $^{238}$U nucleus.

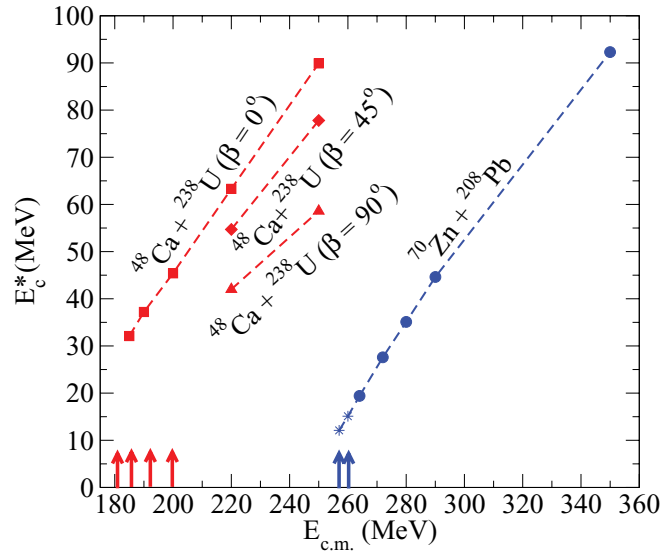


FIG. 3. (Color online) Excitation energy in a central collision at the potential minimum inside the barrier $E_c^*$ as a function of $E_{\text{c.m.}}$ for the $^{48}$Ca + $^{238}$U and the $^{70}$Zn + $^{208}$Pb systems. For the case of the $^{48}$Ca + $^{238}$U system, $^{238}$U alignment angles of $\beta = 0^\circ, 45^\circ, 90^\circ$ are shown.

for which the surface terms vanish at the box boundaries, and calculation of energy-density integrals by assuming a dividing plane would, thus, not be correct).

In Fig. 3, we show the excitation energy as a function of the c.m. energy for both $^{48}$Ca + $^{238}$U and $^{70}$Zn + $^{208}$Pb systems calculated at the potential minimum inside the barrier. The excitation-energy curves increase with a typical linear slope as a function of $E_{\text{c.m.}}$. For the case of the $^{48}$Ca + $^{238}$U system, we show the excitation energies for the $^{238}$U alignment angles of $\beta = 0^\circ, 45^\circ, 90^\circ$. The upward arrows in the bottom of the figure denote the experimental energies for these reactions. For larger alignment angles of $^{238}$U, the curves start at a higher c.m. energy, since at lower energies, we only have deep-inelastic collisions. The lowest two points for the $^{70}$Zn + $^{208}$Pb curve (shown as stars) are simply the extrapolated values down to the experimental energies.

While, at first glance, the excitation energies for the $^{48}$Ca + $^{238}$U system look much higher than those for the $^{70}$Zn + $^{208}$Pb system, this may be somewhat misleading. The reason is that the excitations for the $^{48}$Ca + $^{238}$U system must be angle averaged for different alignments of the $^{238}$U nucleus and must also be weighted by the alignment probability discussed later. So, for example, the $\beta = 0^\circ$ excitation at a particular c.m. energy will be multiplied by the $\sin(\beta)$ factor in the integration weight and will make a zero contribution. The value of $\sin(\beta)$ increases with $\beta$; but, at the same time, the excitation energy decreases. Since TDHF calculations at the experimental energies only yield dinuclear configurations for the small values of $\beta$ but rapidly move into the deep-inelastic domain for larger values, we could not compute this average in practice. Naturally, a fully quantal system will have a certain probability for resulting in a dinuclear configuration for all values of $\sin(\beta)$ at these energies, and the excitation energy will be smaller than the one shown for the $\beta = 0^\circ$ case.

As we have discussed earlier, for systems leading to superheavy formation, the evaporation residue cross section is customarily represented in terms of the various phases of the reaction process as

$$\sigma_{\text{ER}} = \sigma_{\text{capture}}\, P_{\text{CN}}\, P_{\text{survival}}, \tag{5}$$

where $\sigma_{\text{ER}}$ denotes the evaporation residue cross section for the superheavy system, $\sigma_{\text{capture}}$ is the capture cross section for the two ions, $P_{\text{CN}}$ is the probability of forming a compound nucleus, and $P_{\text{survival}}$ is the probability that this compound system survives various breakup and fission events. The calculations presented here can only address the capture cross section for these systems, since the subsequent reaction possibilities are beyond the scope of the TDHF theory. For most light systems for which fusion is the dominant reaction product, $\sigma_{\text{capture}}$ and $\sigma_{\text{ER}}$ are essentially the same and are equal to the fusion cross section $\sigma_{\text{fusion}}$. Instead, for reactions involving superheavy formations, we have

$$\sigma_{\text{capture}} = \sigma_{\text{QF}} + \sigma_{\text{FF}} + \sigma_{\text{ER}}, \tag{6}$$

where $\sigma_{\text{QF}}$ and $\sigma_{\text{FF}}$ denote the quasifission and fusion-fission cross sections, respectively. For these reactions, the evaporation residue cross section $\sigma_{\text{ER}}$ is very small; and, therefore, the capture cross section is, to a large extent, equal to sum of the two fission cross sections. Furthermore, the distinction between deep-inelastic reactions and quasifission is somewhat difficult and, usually, is achieved by setting windows for fragment masses of $A_f = A_{\text{CN}}/2 \pm 20$ and on their kinetic energy.

For the calculation of the capture cross section, we need to average over all possible alignments of the $^{238}$U nucleus

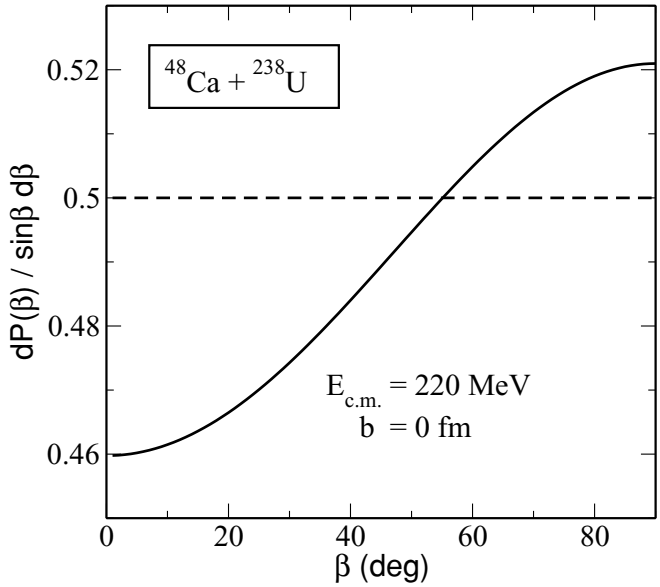


FIG. 4. Dynamic alignment due to Coulomb excitation of $^{238}$U. Shown is the orientation probability as a function of the Euler angle $\beta$ in a central collision at internuclear distances $R = 1500$ fm (dashed horizontal curve) and at $R = 20$ fm at c.m. energy of $E_{\text{c.m.}} = 220$ MeV (solid curve).

[28–32] as given by

$$\sigma_{\text{capture}}(E_{\text{c.m.}}) = \int_0^{\pi} d\beta \, \sin(\beta) \frac{dP}{d\beta \, \sin(\beta)} \sigma(E_{\text{c.m.}}, \beta), \quad (7)$$

where $dP/[d\beta \, \sin(\beta)]$ represents the alignment probability and $\sigma(E_{\text{c.m.}}, \beta)$ is the capture cross section associated with a particular alignment. The TDHF calculations are carried out in a finite 3D box, starting at a finite separation $R$. If one or both nuclei are deformed, we have to generate a series of initial Slater determinants at different orientation angles with respect to the collision axis. The solutions of the static HF equations are independent of orientation in a full 3D calculation. However, different initial orientations naturally result in different collision outcomes in TDHF calculations. As a result of long-range Coulomb excitation, not all initial orientation angles occur with the same probability. Rather, the dominant excitation of the ground-state rotational band in deformed nuclei leads to a preferential alignment, which is calculated in a separate semiclassical Coulomb excitation code [31]. This code is only used to determine the weight factor $dP/d\beta$ in Eq. (7) for the angle averaging of the cross section. Therefore, the Coulex calculation does not impact the Slater determinant.

Due to the relatively small charge of the $^{48}$Ca nucleus, this probability is in the range 0.46–0.52 as shown in Fig. 4 and does not vary appreciably with energy. One important fact to notice in the cross-section formula given in Eq. (7) is that the cross section is multiplied by the $\sin(\beta)$ factor, which renders the contribution originating from the lowest barriers at small values of $\beta$ to be very small. However, unlike the calculation of excitation energy, which requires a TDHF collision at exactly the same experimental energy, the potential barriers are obtained by performing TDHF calculations at higher energies and by using the DC to calculate the ion-ion potentials. For a consistent calculation of fusion cross sections above and below the barrier energies, we have adopted the commonly used incoming wave boundary condition method [33,34]. In practice, we have varied the alignment angle $\beta$ in 10° steps between 0° and 90°. In Fig. 5, we show the capture cross sections for the $^{48}$Ca + $^{238}$U system as a function of $E_{\text{c.m.}}$ energy (black circles). Also shown are the experimental cross sections (red squares) [4].

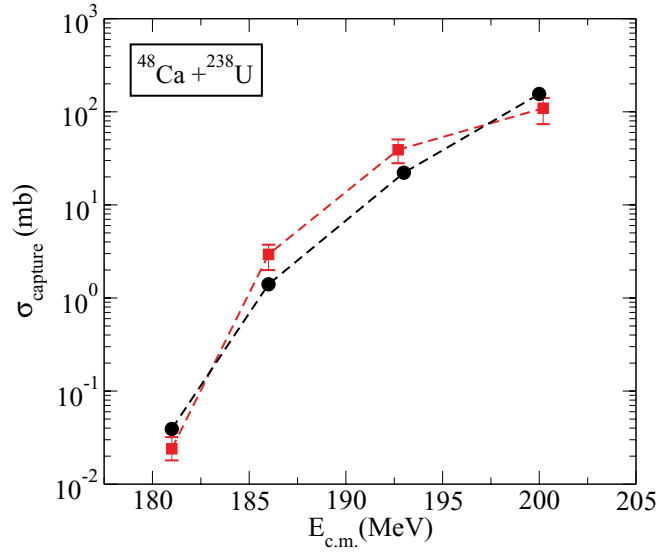


FIG. 5. (Color online) Capture cross sections for the $^{48}$Ca + $^{238}$U system as a function of $E_{\text{c.m.}}$ energy (black circles). Also shown are the experimental cross sections (red squares) [4].

### B. $^{70}$Zn + $^{208}$Pb system

We have also investigated the cold fusion reaction of $^{70}$Zn + $^{208}$Pb, which leads to the same superheavy element $Z = 112$ (but a different isotope). The HF calculations for $^{70}$Zn and $^{208}$Pb produce a spherical nucleus in both cases. In Fig. 6, we plot the potential barriers for the $^{70}$Zn + $^{208}$Pb system obtained from DC-TDHF calculations using Eq. (1) as a function of $E_{\text{c.m.}}$ energy. Also shown is the point Coulomb potential for two spherical nuclei. Unlike light nuclei, the deviations from the Coulomb trajectory start relatively early (15 to 16 fm) due to the large charge of the two ions. A similar behavior to the $^{48}$Ca + $^{238}$U system is observed for the $^{70}$Zn + $^{208}$Pb system, namely, at lower energies, nuclear densities show a dinuclear character for central collisions and result in a deep-inelastic collision at noncentral impact parameters. The lowest barrier in Fig. 6 shows the case at $E_{\text{c.m.}} = 265$ MeV, where even fora central collision, the result is deep inelastic as can be seen from the dotted blue curve. Only for the highest two energies the densities corresponding to central collisions show a more composite character, which be identified as capture, and result in a similar density distribution for noncentral collisions as well. We also observe the flattening of the ion-ion potentials as the nuclear overlap increases at smaller $R$ values, which seems to be a general behavior for collisions of two heavy

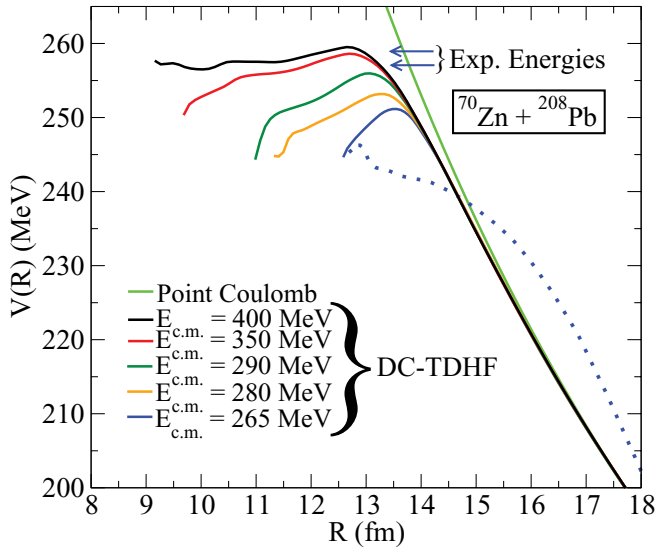


FIG. 6. (Color online) Potential barriers $V(R)$ for the $^{70}$Zn + $^{208}$Pb system obtained from DC-TDHF calculations using Eq. (1) for various $E_{\text{c.m.}}$ energies as indicated.

nuclei. In Fig. 7, we show the excitation energy $E^*(R)$ as a function of the $E_{\text{c.m.}}$ energy for the $^{70}$Zn + $^{208}$Pb system. Again, the highest value attained is at the point where the two nuclei come to a stop inside the ion-ion potential. These energies were shown in Fig. 3 as a function of the $E_{\text{c.m.}}$ energy.

We have also calculated the capture cross section for the $^{70}$Zn + $^{208}$Pb system. Since we are dealing with two spherical nuclei, no angle averaging is necessary for this system. However, we could not find experimental measurements for the capture cross section. For comparison, we have used a model calculation where the cross sections for the synthesis of superheavy elements were analyzed using the concept of a dinuclear system [29]. The authors calculated capture or quasifission, fusion, and $1n$ evaporation residue cross sections, which reproduced a single $1n$ evaporation residue experimental cross

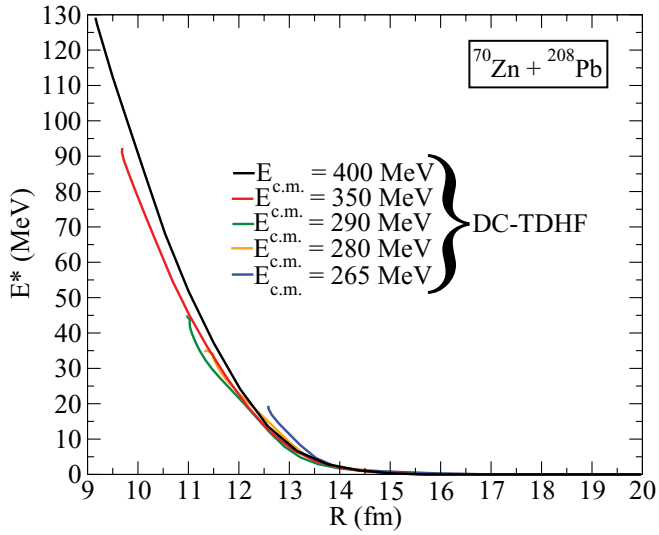


FIG. 7. (Color online) Excitation energy $E^*(R)$ for the $^{70}$Zn + $^{208}$Pb system and for various $E_{\text{c.m.}}$ energies as indicated.

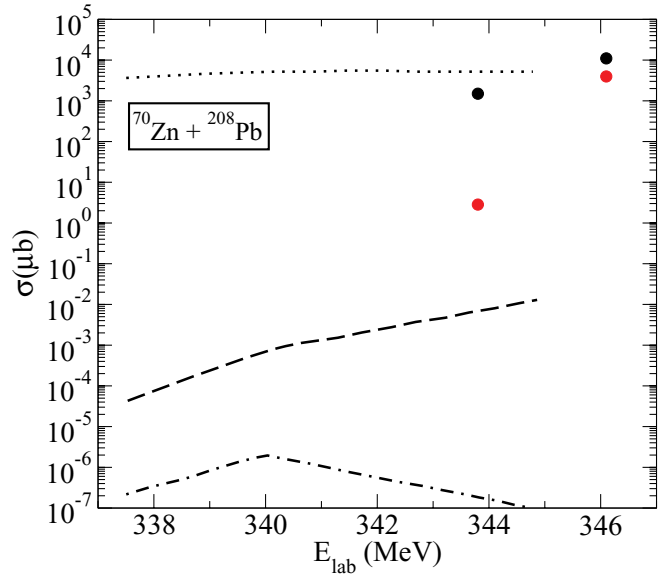


FIG. 8. (Color online) Cross sections (in microbarns) from Ref. [29] as a function of the $E_{\text{lab}}$ energy for the $^{70}$Zn + $^{208}$Pb system. The dotted curve shows the quasifission, the dashed curve shows the fusion, and the dotted-dashed curve shows the $1n$ evaporation residue cross section. Our calculations for the two experimental energies corresponding to the two potential energies leading to capture in Fig. 6 are shown as filled circles.

section. For comparison, we have plotted our capture cross sections together with their findings for the two experimental laboratory energies [2] of $E_{\text{lab}} = 343.8$ MeV and 346.1 MeV in Fig. 8. Our calculations at the two experimental energies corresponding to the two potential energy curves leading to capture in Fig. 6 are shown as filled circles. Differences in laboratory energies between our results and the results of the model calculation [29] stem from the fact that model calculations make use of the compound-nucleus excitation energy and relate this to the laboratory energy. We have directly used the experimental energies from Ref. [2], since we do not compute the compound-nucleus excitation energy. On the other hand, the dependence of the quasifission cross section on laboratory energy is very flat as shown in Fig. 8. As we can see, the calculated cross sections at the higher laboratory energy of 346.1 MeV is in reasonable agreement with the model calculation for both potential-energy curves, whereas for the lower laboratory energy of 343.8 MeV, the lower potential-energy curve substantially underestimates the model calculation. We may conclude, from this observation, that the higher potential-energy curve provides a better representation of the inner part of the ion-ion barrier. However, since we cannot rule out the lower potential-energy curve as a capture event based on our TDHF results, we have shown both results.

Finally, for the calculation of capture cross sections, it is possible to use a coordinate-dependent effective mass $\mu(R)$ as described in Ref. [21]. The effect of using a coordinate-dependent mass is to modify the inner part of the ion-ion potential, particularly at low subbarrier energies. For the energies studied here, we have found this effect to be very small for capture cross sections.

## IV. SUMMARY

In this work, we have investigated two systems, which are known to produce the element $Z = 112$ in experiments. We find that the collisions of such heavy systems have very different characteristics than the TDHF calculations of light- and medium-mass systems. We have used the DC along with the TDHF to obtain ion-ion interaction potentials and excitation energies. The dependence of the ion-ion potential on the deformation of the $^{238}$U nucleus was studied. The calculated capture cross sections are found to be in reasonable agreement with data and other model calculations. However, since the DC-TDHF potential is obtained by TDHF calculations at above barrier energies, the intrinsic excitation process during tunneling is not considered, which may also play a role in capture probability.

The fully microscopic TDHF theory has shown itself to be rich in nuclear phenomena and continues to stimulate our understanding of nuclear dynamics. The time-dependent mean-field studies seem to show that the dynamic evolution builds up correlations that are not present in the static theory. While modern Skyrme forces provide a much better description of static nuclear properties in comparison to the earlier parametrizations, there is a need to obtain even better parametrizations that incorporate deformation and scattering data into the fit process.

## ACKNOWLEDGMENTS

This work has been supported by the US Department of Energy under Grant No. DE-FG02-96ER40963 with Vanderbilt University, and by the German BMBF under Contracts No. 06F131 and No. 06ER142D. One of us (A.S.U.) acknowledges the support of the Hessian LOEWE initiative through the Helmholtz International Center for FAIR (HICforFAIR) during his stay in Frankfurt.

[1] S. Hofmann and G. Münzenberg, Rev. Mod. Phys. **72**, 733 (2000).
[2] S. Hofmann *et al.*, Eur. Phys. J. A **14**, 147 (2002).
[3] Y. T. Oganessian *et al.*, Phys. Rev. C **70**, 064609 (2004).
[4] Y. Oganessian, J. Phys. G **34**, R165 (2007).
[5] S. Hofmann *et al.*, Eur. Phys. J. A **32**, 251 (2007).
[6] G. Fazio *et al.*, Eur. Phys. J. A **19**, 89 (2004).
[7] G. Fazio *et al.*, Phys. Rev. C **72**, 064614 (2005).
[8] G. G. Adamian, N. V. Antonenko, and W. Scheid, Phys. Rev. C **68**, 034601 (2003).
[9] A. K. Nasirov, G. Giardina, G. Mandaglio, M. Manganaro, F. Hanappe, S. Heinz, S. Hofmann, A. I. Muminov, and W. Scheid, Phys. Rev. C **79**, 024606 (2009).
[10] G. G. Adamian, N. V. Antonenko, and W. Scheid, Eur. Phys. J. A **41**, 235 (2009).
[11] Z.-Q. Feng, G.-M. Jin, J.-Q. Li, and W. Scheid, Nucl. Phys. A **816**, 33 (2009).
[12] J. C. Pei, W. Nazarewicz, J. A. Sheikh, and A. K. Kerman, Phys. Rev. Lett. **102**, 192501 (2009).
[13] J. W. Negele, Rev. Mod. Phys. **54**, 913 (1982).
[14] Lu Guo, J. A. Maruhn, P.-G. Reinhard, and Y. Hashimoto, Phys. Rev. C **77**, 041301(R) (2008).
[15] A. S. Umar and V. E. Oberacker, J. Phys. G **36**, 025101 (2009).
[16] A. S. Umar, V. E. Oberacker, and J. A. Maruhn, Eur. Phys. J. A **37**, 245 (2008).
[17] A. S. Umar and V. E. Oberacker, Phys. Rev. C **74**, 021601(R) (2006).
[18] R. Y. Cusson, P.-G. Reinhard, M. R. Strayer, J. A. Maruhn, and W. Greiner, Z. Phys. A **320**, 475 (1985).
[19] A. S. Umar and V. E. Oberacker, Phys. Rev. C **74**, 061601(R) (2006).
[20] A. S. Umar and V. E. Oberacker, Phys. Rev. C **77**, 064605 (2008).
[21] A. S. Umar and V. E. Oberacker, Eur. Phys. J. A **39**, 243 (2009).
[22] K. Washiyama, D. Lacroix, and S. Ayik, Phys. Rev. C **79**, 024609 (2009).
[23] A. S. Umar, V. E. Oberacker, J. A. Maruhn, and P.-G. Reinhard, Phys. Rev. C **80**, 041601(R) (2009).
[24] W. Swiatecki, Nucl. Phys. A **376**, 275 (1982).
[25] C. Simenel, B. Avez, and C. Golabek, arXiv:0904.2653.
[26] E. Chabanat, P. Bonche, P. Haensel, J. Meyer, and R. Schaeffer, Nucl. Phys. A **635**, 231 (1998); **643**, 441(E) (1998).
[27] A. S. Umar and V. E. Oberacker, Phys. Rev. C **73**, 054607 (2006).
[28] V. Y. Denisov and S. Hofmann, Phys. Rev. C **61**, 034606 (2000).
[29] G. Giardina, S. Hofmann, A. I. Muminov, and A. K. Nasirov, Eur. Phys. J. A **8**, 205 (2000).
[30] V. Y. Denisov and W. Nörenberg, Eur. Phys. J. A **15**, 375 (2002).
[31] A. S. Umar and V. E. Oberacker, Phys. Rev. C **74**, 024606 (2006).
[32] R. K. Gupta, Niyti, M. Manhas, S. Hofmann, and W. Greiner, Int. J. Mod. Phys. E **18**, 601 (2009).
[33] G. H. Rawitscher, Phys. Rev. **135**, 605 (1964).
[34] S. Landowne and S. C. Pieper, Phys. Rev. C **29**, 1352 (1984).